



# Multi-channel Singular Spectrum Analysis of Geocenter Motion and Precise Prediction of Earth's Motion

Xin Jin<sup>1</sup>, Xin Liu<sup>1</sup>(✉), Jinyun Guo<sup>1</sup>, and Yi Shen<sup>2</sup>

<sup>1</sup> College of Geodesy and Geomatics, Shandong University of Science and Technology, Qingdao 266590, China

skd994268@sdust.edu.cn

<sup>2</sup> School of Geographic Sciences, Xinyang Normal University, Xinyang 464000, China

**Abstract.** Geocenter is the center of the mass of the Earth system including the solid Earth, ocean and atmosphere. The time-varying characteristics of geocenter motion (GCM) can reflect the redistribution of the Earth's mass and the interaction between solid Earth and mass loading. The GCM also provides important support for millimeter level, dynamic real-time global reference framework. The GCM products determined from satellite laser ranging data released by the Center for Space Research through Jan. 1993 to Feb. 2017 is utilized to determine the periods and the long-term trend of GCM by using multi-channel singular spectrum analysis (MSSA). The results show that the GCM has the amplitude between 1 mm and 10 mm, and has obvious seasonal characteristics of the annual, semiannual, quasi-0.6 years and quasi-1.5 years in X, Y and Z directions, the annual characteristics make great domination. It also shows long period terms of 6.09 years as well as the trends of 0.05 mm/yr, 0.04 mm/yr and  $-0.10$  mm/yr in the three directions, respectively. The MSSA is applied to predict GCM and combines it with the linear model (LM) and autoregressive moving average model (ARMA) to predict GCM with ahead 2 years. The results show that the LM+MSSA+ARMA model can effectively predict GCM parameters, and can provide prediction precision of 1.5 mm, 1.1 mm and 3.5 mm in X, Y and Z directions, respectively.

**Keywords:** Multi-channel singular spectrum analysis · Geocenter motion · Prediction · ARMA

## 1 Introduction

The center of mass (CM) of the Earth is defined as the center of the mass of the entire Earth including solid Earth, ocean and atmosphere (Montag 1999; Pavlis 1999) (see Table 1 for a list of abbreviations used in the paper). Sea level change, glacier melting, atmospheric circulation, and mantle convection result in the CM movement relative to the center of the figure (CF) of the Earth surface, which reflects the global mass redistribution and the interaction between solid Earth and mass loading (Wu et al. 2012; Cheng et al. 2013a). The geocenter motion (GCM) is helpful to study the problem that

the International Terrestrial Reference Frame (ITRF) implementation is not completely consistent with the International Terrestrial Reference System (ITRS) definition, which will further improve the precision of the reference frame origin (Blewitt 2003; Dong et al. 2003; Metivier et al. 2010; Altamimi et al. 2011). The GCM has an important impact on the reference frame transformation of Satellite Laser Ranging (SLR), Global Navigation Satellite System (GNSS) and Doppler Orbitography and Radio-positioning Integrated by Satellite (DORIS) system (Wei et al. 2016; Riddell et al. 2017). It is also an important topic for studying the Earth's mass redistribution, such as ocean tide, glacial isostatic adjustment, atmospheric and ocean circulation, geodynamic process in the Earth's interior (Trupin et al. 1992; Dong et al. 1997; Watkins and Eanes 1997).

**Table 1.** Abbreviations used in this paper

Acronym	Full name	Acronym	Full name
CM	Center of the mass	ITRS	International Terrestrial Reference System
CF	Center of the figure	SLR	Satellite Laser Ranging
GCM	Geocenter motion	GNSS	Global Navigation Satellite System
CSR	Center for Space Research	DORIS	Doppler Orbitography and Radio-positioning Integrated by Satellite
MSSA	Multi-channel singular spectrum analysis	IGS	International GNSS Service
SSA	Singular spectrum analysis	GRACE	Gravity Recovery and Climate Experiment
LM	Linear model	UTOPIA	University of Texas Orbit Determination Program
ARMA	Autoregressive moving average model	LLISS	Large Linear System Solver
ITRF	International Terrestrial Reference Frame		

SLR data were processed to estimate effectively GCM (Bouille et al. 2000; Crétaux et al. 2002). The fewer SLR sites, the maldistribution of sites and the absence of SLR data on the ocean lead to the deterioration of the measurement precision. GNSS data were also used to determine GCM (Blewitt and Clarke 2003). Although there are more International GNSS Service (IGS) stations all over the world, GNSS satellite orbital altitude is so high that the precision of GNSS-derived GCM is lower than that of SLR-derived products. The DORIS-derived GCM in Z direction is very different from the other two directions and its precision is only up to centimeter-level. DORIS-derived GCM has the lowest precision among the series estimated by these three space geodetic techniques (Kuzin and Tatevian 2005; Kong et al. 2017). The time series of GCM in

different time-span can be accurately estimated by using the SLR data of Lageos-1, Lageos-2 and other geodynamical satellites.

The wavelet transformation, least squares spectral analysis, singular spectrum analysis (SSA) can be used to discover the characteristics of GCM in X, Y and Z directions (Guo et al. 2009; Wei et al. 2016). However, when analyzing the GCM, these methods cannot take into account the correlation of all directions of GCM. Multi-channel singular spectrum analysis (MSSA), as the extended form of SSA, is one of the effective statistical data analysis methods in oceanography, geoscience, meteorology and other fields (Vautard and Ghil 1989; Wang et al. 2016; Zotov et al. 2016; Zhou et al. 2018). The MSSA is a method for analyzing nonlinear time series. It is also able to denoise data, extract periodic oscillation signals, identify trends from multidimensional time series and build prediction models (Shen et al. 2017, 2018). Compared with SSA, during the process of multidimensional time series, the correlations among different channels are taken into account, so we apply the MSSA method to the analysis of GCM and study the ability to extract periodic signals of GCM.

The monitoring and modeling of GCM is a key issue for constructing a millimeter-level, dynamic and real-time global reference frame. However, due to the complexity of obtaining multi-source observations and data processing, The GCM parameters cannot be obtained in real-time or quasi-real-time (Altamimi et al. 2011; Zhao et al. 2019). Therefore, the MSSA model is applied to predict GCM parameters and proposes a GCM prediction method that combines linear model (LM), MSSA and autoregressive moving average model (ARMA).

SLR-derived GCM series from Jan. 1993 to Feb. 2017 updated by the Center for Space Research (CSR), the Texas University at Austin, are used to study GCM variation in this paper. The trend and periodic variations of GCM are investigated by using MSSA. Finally, based on historical GCM data, the fusion method of LM, MSSA and ARMA models is used to predict GCM parameters.

## 2 Data Collection and Methodology

### 2.1 SLR-Derived GCM Products

The GCM products used in this paper are obtained from CSR at University of Texas website (<http://ftp.csr.utexas.edu/pub/slr/geocenter/>). The GCM products (GCN\_L1\_L2\_30d\_CF-CM) were solved with UTOPIA and LLISS from SLR data of geodynamical satellites (e.g. Lageos-1/2, Starlette, Ajisai and Stella) in SLRF2014 (Cheng et al. 2013a; Pearlman et al. 2019). CF-CM is intended to reflect the true degree-1 mass variations without being affected by the higher-degree site loading effects (particularly at the annual frequency) (Ries 2016). The GCM products are often used to study the local and global mass balance with GRACE and are currently the best geocenter coordinate result recognized internationally. Here we download the GCM products from Jan. 1993 to Feb. 2017.

## 2.2 Multi-channel Singular Spectrum Analysis

There is a time series  $x_{li}$  ( $l = 1, \dots, L$ ;  $i = 1, \dots, N$ ) in which  $l$  is channel number and  $i$  is time sequence number. The rank of  $x_{li}$  is arranged according to the time delay phase space  $M$  ( $1 \leq M \leq N/2$ ) that is the window length and also called the step number of time lag. The integer multiple of the main cycle is generally chosen as one window length in MSSA (Oropeza and Sacchi 2011; Shen et al. 2018).

The trajectory matrix of the channel  $l$  is

$$\mathbf{X}_i = \begin{bmatrix} x_{1i} & x_{2i} & \cdots & x_{Ki} \\ x_{2i} & x_{3i} & \cdots & x_{K+1i} \\ \vdots & \vdots & \vdots & \vdots \\ x_{Mi} & x_{M+1i} & \cdots & x_{Li} \end{bmatrix} \quad (1 \leq i \leq N) \quad (1)$$

where  $K = N - M + 1$ . The multi-channel trajectory matrix can be indicated as

$$\mathbf{X} = [\mathbf{X}_1, \mathbf{X}_2, \dots, \mathbf{X}_N]^T \quad (2)$$

Matrix  $\mathbf{X}$  has  $L \times M$  rows and  $N - M + 1$  columns. Similar to SSA, the next step is to decompose the singular value of  $\mathbf{X}$ . We define the matrix  $\mathbf{S} = \mathbf{X}\mathbf{X}^T$ , where  $\mathbf{X}^T$  is the transposed matrix of  $\mathbf{X}$ . Suppose that  $\lambda_1, \dots, \lambda_M$  are the eigenvalues of matrix  $\mathbf{S}$ , that is, the singular values. These eigenvalues are arranged in the descending order. The larger singular value generally represents the larger energy signal and the smaller one corresponds to the noise part. Matrix  $\mathbf{X}$  can be expressed in the elementary matrix as

$$\mathbf{X} = \mathbf{P}_1 + \mathbf{P}_2 + \cdots + \mathbf{P}_D \quad (3)$$

where  $D$  represents the number of singular values, and  $\mathbf{P}_i = \mathbf{S}_i \mathbf{U}_i \mathbf{V}_i^T$  in which  $\mathbf{U}_i$  is the temporal empirical orthogonal function and  $\mathbf{V}_i$  is the temporal principal components.

The GCM time series contain different signals, such as annual term and semi-annual term. It is necessary to use the w-correlation method (Hassani 2007) to merge elementary matrix  $\mathbf{P}_i$  representing the same signal into a group. Suppose that the time series after reconstruction of each elementary matrix  $\mathbf{P}_i$  is  $\mathbf{Y}_i$ , the correlation of any two reconstructed time series can be expressed by w-correlation as

$$\rho_{i,j}^w = \frac{(Y^{(i)}, Y^{(j)})}{\|Y^i\|_w \|Y^j\|_w}, \quad (1 \leq i, j \leq L) \quad (4)$$

Where  $\|Y^i\|_w = \sqrt{(Y^{(i)}, Y^{(i)})}$ ,  $(Y^{(i)}, Y^{(j)}) = \sum_{k=1}^N w_k y_k^i y_k^j$ , and  $w_k = \min(k, M, N - k)$ .

The larger the absolute value of  $\rho_{i,j}^w$  is, the greater the correlation of the corresponding components of  $i$  and  $j$  is, which should be classified as the same periodic signal component. Then the corresponding trajectory matrix has been build.

The corresponding group of trajectory matrix is converted into a new time series with the length of  $N$ , which is called the reconstructed component (Golyandina et al. 2001). Then the reconstructed component (RC) is

$$x_{li}^k = \begin{cases} \frac{1}{i} \sum_{j=1}^i a_{i-j}^k E_{lj}^k & 1 \leq i \leq M - 1 \\ \frac{1}{M} \sum_{j=1}^M a_{i-j}^k E_{lj}^k & M \leq i \leq N - M + 1 \\ \frac{1}{N-i+1} \sum_{j=i-N+M}^M a_{i-j}^k E_{lj}^k & N - M + 2 < i \leq N \end{cases} \quad (5)$$

### 3 Analysis of GCM

#### 3.1 GCM Seasonal Variation

The GCM time series comprising monthly data ( $L = 290$ ) from Jan. 1993 to Feb. 2017 are used to analyze GCM variation. The trajectory matrix of GCM are decomposed by selecting the window  $M = 108$  (month), which is determined by the period of the annual term of GCM and many practical experiments. Singular values in descending order are shown in Fig. 1.

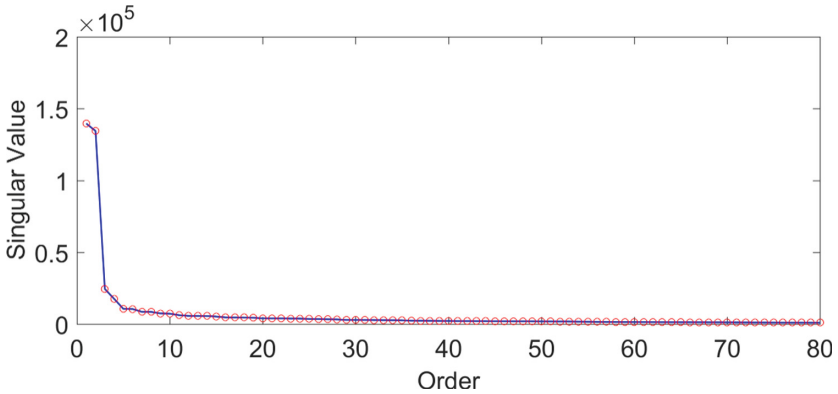


**Fig. 1.** Singular values of GCM series determined by MSSA

As shown in Fig. 1 that the values starting from the 20th singular value are already smaller than the first 4th previous singular values, and the values after 20th order change smoothly so that they can be ignored. The w-correlations  $\rho_{i,j}^w$  of the first 20 reconstruction parts of GCM in the three directions except for the trend term are shown in Fig. 2.

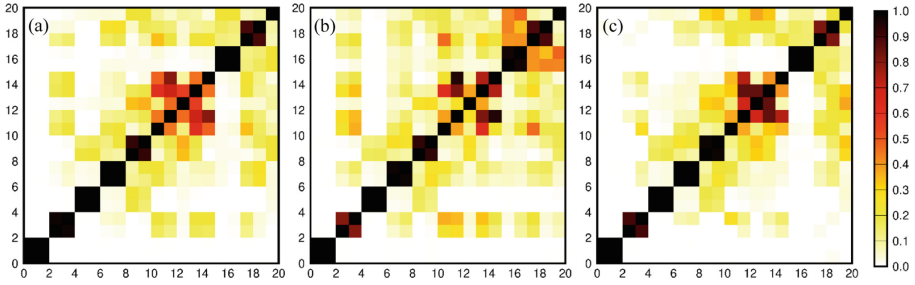


**Fig. 2.** W-correlations for the first 20 reconstructions. (a) X direction, (b) Y direction, and (c) Z direction.

The greater w-correlation  $\rho_{i,j}^w$  means the corresponding components belong to the same periodic term. As shown in Fig. 2 that the time series in the X direction is not completely separated from each other when  $i > 10$  and the separation effect in both Y and Z directions also deteriorates after  $i > 10$ , which may be caused by noises. Hence, the first 10 groups (RC1, RC2, ..., and RC10) are used to reconstruct the new GCM series. RC1 and RC2 represent a periodic term in the original series; RC3 and RC4 represent the other one; RC5 and RC6, RC7 and RC8, RC9 and RC10 can be combined into one periodic component, respectively. Figure 3 shows the original GCM series in X, Y and Z directions except for the trend term and the time series reconstructed by the first 10-order reconstruction components.

As shown in Fig. 3 that the fluctuation ranges of raw GCM in X and Y directions are smaller than that in Z direction. Although the offset of CM relative to CF in the Z direction is large, the fluctuation amplitude is small, and most of them are negative.

The correlation coefficients between the time series reconstructed by the first 10 singular vectors and the corresponding original time series in X, Y and Z directions are 73.34%, 86.78% and 83.84%, respectively, which indicates that they have good consistency. It shows that MSSA model can effectively extract relatively complete information about the main components in the three directions.

Table 2 shows the singular spectrum values and the variance contributions of GCM time series calculated by MSSA from 1993 to Feb. 2017. The variance contribution of the first 10-order reconstruction components has reached 65.80%, which can characterize the variation of GCM effectively. Furthermore, the variance contribution of reconstruction RC1 and RC2 is significantly larger than that of other components, which indicates that the corresponding cyclophysis is most obvious. The first 10-order reconstruction components can be combined into five periodic terms according to the principle of w-correlation. Figures 4, 5 and 6 show the reconstructed component and the corresponding power spectrum in the three directions.

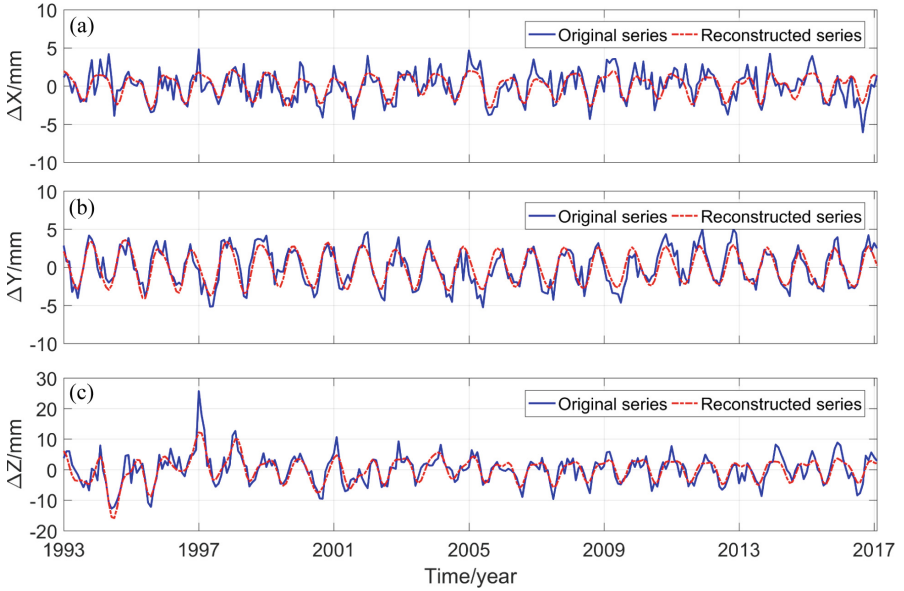


**Fig. 3.** Time series of GCM from 1993 to 2017.2. (a) X direction, (b) Y direction, and (c) Z direction.

**Table 2.** Singular values and variance contributions of the first 10 orders based on MSSA

Order/RC	Singular spectrum value	Variance contribution
1	139651.7	24.90%
2	134495.7	23.98%
3	24465	4.36%
4	17625.2	3.14%
5	10608.3	1.89%
6	10477.4	1.87%
7	8517.8	1.52%
8	8476.8	1.51%
9	7423.4	1.32%
10	7285.8	1.30%

As shown in Figs. 4, 5 and 6 that the five main periodic terms of GCM in three directions are basically the same. There is the annual term, semi-annual term, quasi-0.6 years term, quasi-1.5 years term and long-term term. The cycles are respectively 0.99 years, 0.5 years, 0.58 years, 1.47 years and 6.09 years. The fifth main periodic term is also mixed with a small periodic term of about 1.4 years. The variance contributions

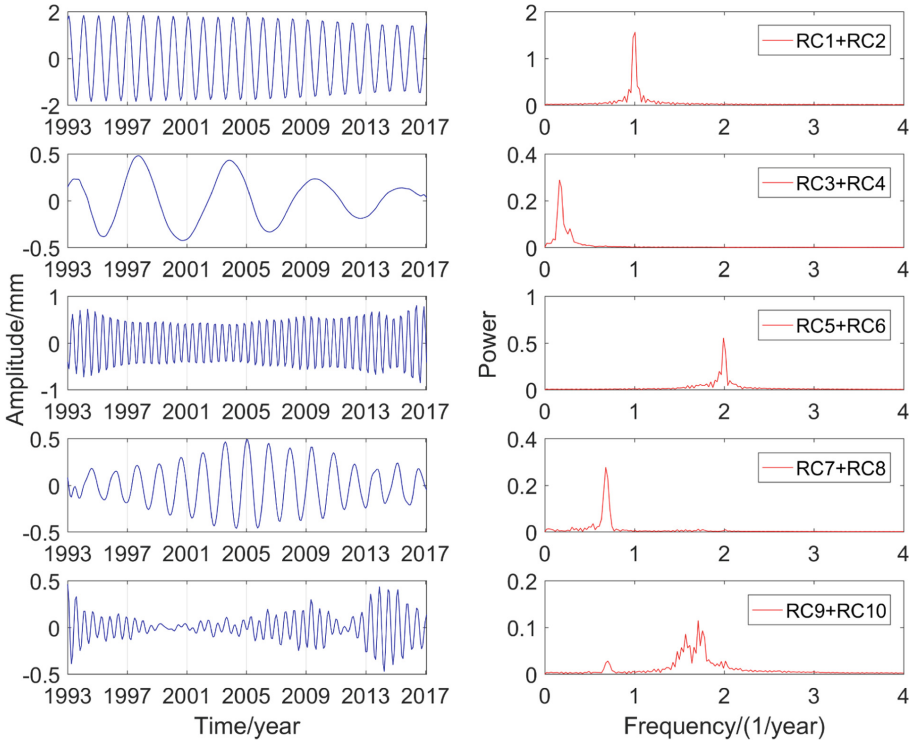


**Fig. 4.** Combination of RC and the power spectrum analysis in X direction

of these five main periodic components in the three directions are different, and annual characteristics make great domination.

The annual periodic oscillations in the three directions are relatively stable, and the periodicity is the most obvious, with amplitudes of about 1.7 mm, 2.8 mm and 4.4 mm respectively. The valley value of the annual variation of GCM in X direction occurs from August to September and the peak value appears from February to March. The valley value of the annual variation of GCM in Y direction occurs from May to June and the peak value appears from November to December. The valley value of the annual variation of GCM in Z direction occurs from July to August and the peak value appears from January to February. The semi-annual term oscillation is not relatively obvious. Although the semi-annual variations of 0.5 years are shown in these three directions, the corresponding amplitude variation characteristics are not the same. In the past decade, the amplitude of the semi-annual cycle in three directions have gradually increased. The cyclophysis of quasi-1.5 years and quasi-0.6 years, one of the five main periods of GCM, also exhibits strong seasonal characteristics. The oscillation characteristics of quasi-1.5 years and quasi-0.6 years period in Y and Z direction are similar, and the amplitude gradually decreases with time. The oscillation of quasi-1.5 years period in X direction has obvious fluctuations and reached its maximum in February 2005. The



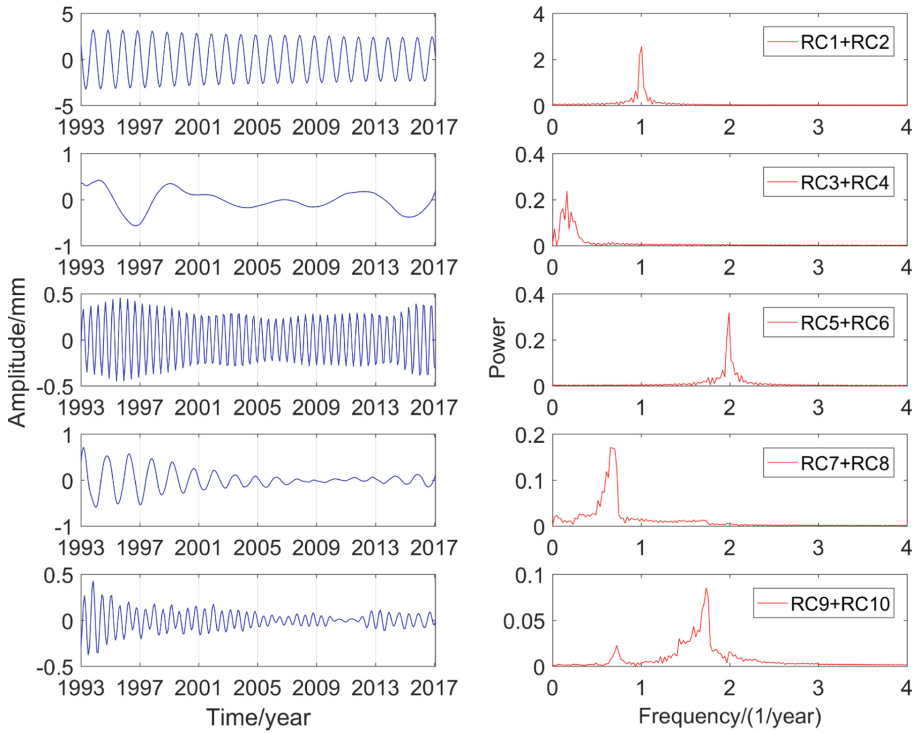


**Fig. 5.** Combination of RC and the power spectrum analysis in Y direction

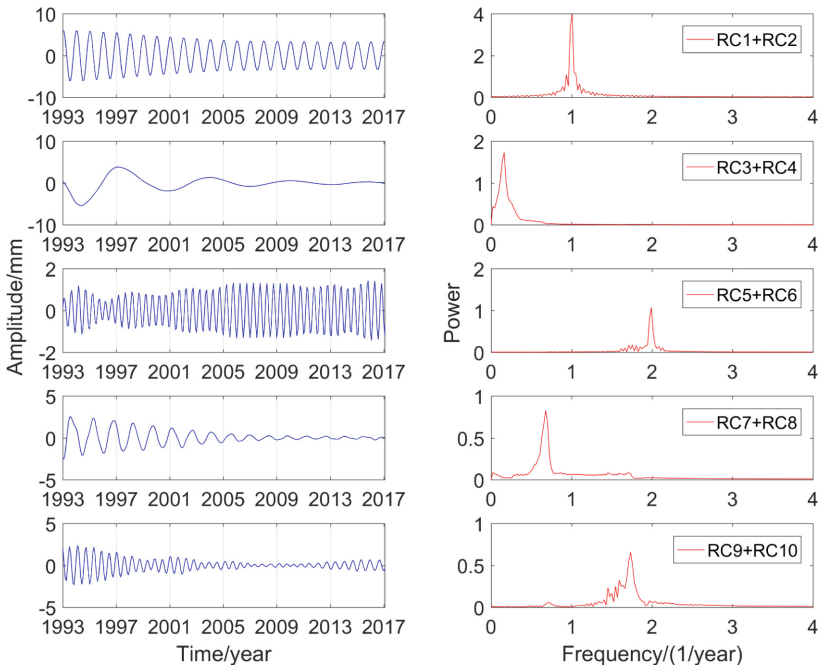


**Fig. 6.** Combination of RC and the power spectrum analysis in Z direction

seasonal characteristic of the quasi-0.6 years period in X direction is obvious, which may be due to the inclusion of many other signals in the period.

The annual term, semi-annual term, quasi-0.6 years term and quasi-1.5 years term mentioned above belong to the seasonal cycle of GCM. The solar radiation, changes in the gravitational field and other Earth external energy cause the surface mass redistribution of land water, ocean and atmosphere, which results in the significant seasonal GCM. The major reason for the seasonal cycle of GCM is the seasonal variation of land water storage (Guo et al. 2008; Feissel-Vernier et al. 2006). The exchange of water mass in the Earth's hemisphere has a clear annual cycle. Greater water mass in the northern hemisphere appears during June-August, instead of appears during December-February in the southern hemisphere (Blewitt et al. 2001; Baur et al. 2013). The peak and valley values of the annual term in Z direction may be the reflection of water mass redistribution.

The long period terms in X, Y and Z directions analyzed by MSSA are all 6.09 years. The major reason for the secular variation of center of mass of the Earth system is the glacial isostatic adjustment. The influence of the glacial ablation on the solid Earth causes GCM velocity of less than 1 mm/yr (Klemann and Martinec 2011). The amplitude of the long-period term in the X direction is maintained within 0.5 mm, but the amplitude in the Y and Z directions has a sudden increase of 1 mm in 1997, which may be caused by the El Niño that was strongest in the 20th century (Guo et al. 2009).

### 3.2 GCM Trend Variation

The GCM series in X, Y and Z directions are directly decomposed and analyzed by using MSSA to determine their trends. The GCM trend variation from 1993 to 2017.2 is shown in Fig. 7. The secular velocity of GCM is calculated by least square method. Table 3 shows the comparisons among the proposed method and the reported methods.

As shown in Fig. 7 that the trend variation in the three directions of GCM are nonlinear. After 1997, the moving direction of GCM in the three directions remained stable. It can be seen from Table 3 that the long-term speed of GCM obtained from different data and time has a relatively large difference, and there is no accurate reference standard at present. In this paper, the variation rates in X, Y and Z are 0.05 mm/yr, 0.04 mm/yr and  $-0.10$  mm/yr, respectively, all of which are less than 1 mm/yr. After 1997, the long-term variation rate of GCM in Z direction is negative, which may be caused by glacial isostatic adjustment (Wu et al. 2010).

Due to the local expansion of the zero-degree hemisphere and the condensation of the 180-degree hemisphere, the variation rate of GCM in X direction is positive, which shows that CM moves towards the X direction relative to CF. Besides, the maximum variation of atmospheric pressure occurs in Central Asia (Blewitt et al. 2001; Greff-Lefftz and Legros 2007). The solid Earth is a viscous elastomer so that the maximum fluctuation of atmospheric pressure in Central Asia may have a certain impact on GCM in Y direction, which results in the positive of the secular velocity.

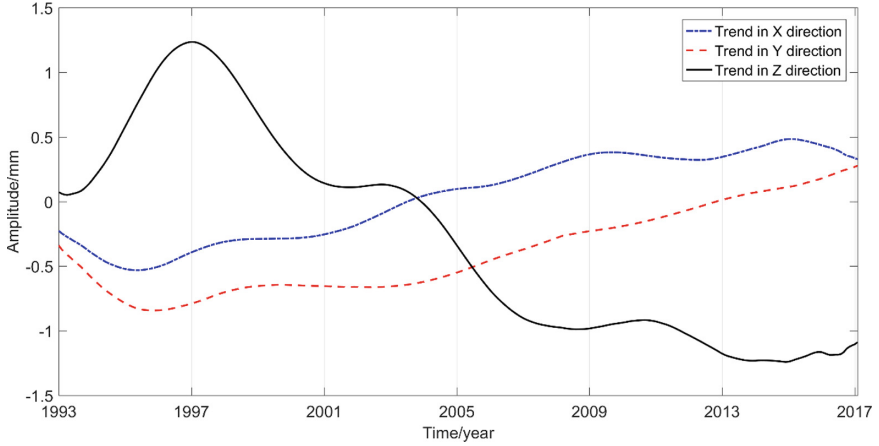


**Fig. 7.** GCM trend variation by using MSSA

**Table 3.** Secular velocity of GCM in different studies (mm/yr)

Literature	Data and model	X	Y	Z	Time span
This paper	SLR	$0.05 \pm 0.003$	$0.04 \pm 0.004$	$-0.10 \pm 0.01$	1993–2017.2
Guo et al. (2009)	SLR	$-0.26 \pm 0.02$	$0.43 \pm 0.02$	$0.50 \pm 0.02$	1993–2006
Kuzin et al. (2010)	DORIS/INA	$-1.19 \pm 0.07$	$-0.12 \pm 0.07$	$-0.28 \pm 0.31$	1993–2009
Rietbroek et al. (2012a)	GRACE/Jason-1/GIA	-0.28	0.43	-1.08	2003–2008
Sun et al. (2016)	GRACE/OMCT/ICE-5G_VM2	$-0.03 \pm 0.03$	$0.11 \pm 0.02$	$-0.21 \pm 0.04$	2002.6–2014.5
Sun et al. (2016)	GRACE/OMCT/ICE-6G_VM5a	$-0.06 \pm 0.03$	$0.07 \pm 0.02$	$-0.33 \pm 0.04$	2002.6–2014.5

## 4 Prediction of GCM

### 4.1 Principle of Prediction

With the continuous development and improvement of space technology, there is a growing demand for the prediction parameters of GCM, such as millimeter level, dynamic real-time global reference framework and high-precision satellite navigation and positioning (Metivier et al. 2010; Zhao et al. 2019). To meet this demand, therefore, the combined method of LM and MSSA and ARMA is applied to predict the GCM parameters. The flow chart of prediction is shown in Fig. 8.

- (1) First, perform linear fitting on the GCM series, establish a linear model and make predictions. Assuming that the GCM time series is  $X_t$ , the least squares method is used to linearly fit it, and the model is expressed as:

$$X_t = \beta_0 + \beta_1 t \quad (6)$$

Where  $\beta_0$  is a constant, and  $\beta_1$  represents the linear trend change rate.

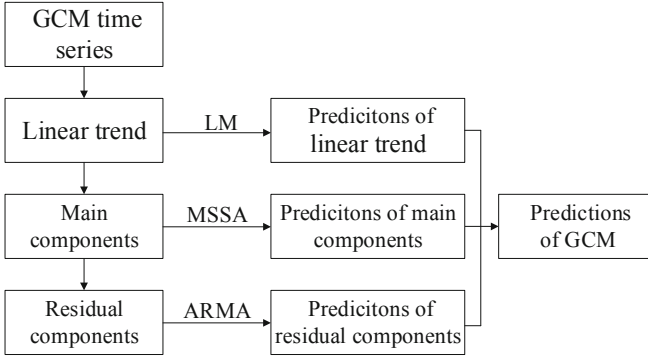


**Fig. 8.** The prediction method of GCM

(2) MSSA is used to decompose the GCM series of the de-linear trend, and the appropriate main component terms are selected for the main component prediction of the GCM. The main component prediction method of MSSA is as follows:

- The number of predictions of GCM is  $N$ , assuming that the time series of GCM without linear trend is  $Y_t$ ,  $N$  zeros are added at the end of  $Y_t$  to form a new prediction sequence  $Y_{t+N}$ ;
- The new prediction sequence  $Y_{t+N}$  is decomposed by MSSA, and the  $N$  values at the end of the first RC (RC1) are used to replace the corresponding prediction values of the new sequence. This process is repeated until the RMS value of the two replacements data is less than 0.001 mas;
- RC2 is added to reconstruct the prediction data, that is, the prediction data is obtained by linear superposition of RC1 and RC2. Step 2 is repeated until RC1...RCi is linearly added to the prediction data, and the predictions using MSSA can be obtained.

(3) ARMA is used to model and forecast the residual components reconstructed by MSSA. Assuming that the sequence of residual items is  $Z_t$ , the ARMA model is expressed as:

$$Z_t = c + \sum_{i=1}^p \phi_i Z_{t-i} + \varepsilon_t + \sum_{j=1}^q \theta_j \varepsilon_{t-j} \quad (7)$$

Where  $p$  represents the order of the AR model,  $q$  represents the order of the MA model,  $c$  is the constant term of the ARMA model,  $\phi_i$  is the free regression coefficient at time  $t - i$ ,  $\varepsilon_t$  is the error term at time  $t$ , and  $\theta_j$  is the moving average coefficient at time  $t - j$ . The extended autocorrelation function (EACF) is selected to determine the order  $p$  and  $q$  of the AR model and the MA model through the maximum likelihood estimation method. The model parameters are estimated to build the ARMA model and predict the residual items.

Finally, the GCM predictions are obtained by adding the predictions of the linear model, MSSA and ARMA models.

## 4.2 Results and Analysis

This paper selects the time series of GCM from 1993 to Feb. 2017 provided by CSR for prediction research. Taking the data from January 1993 to the starting time of forecast as the training data, seven 2-year forecast experiments were carried out. The starting time was January, May and September 2013, January, May and September 2014 and January 2015, respectively. Through the analysis in Sect. 3, the MSSA window and main component were selected as 108 and 10. Through EACF analysis, it is found that ARMA(0,6), ARMA(0,11) and ARMA(3,9) have good applicability to the residual items in the X, Y and Z directions of GCM, respectively.

**Table 4.** The statistical precision of LM+MSSA+ARMA model (mm)

Lead prediction	6 month			12 month			24 month		
	X	Y	Z	X	Y	Z	X	Y	Z
Max	2.92	1.53	7.11	3.28	2.34	7.11	3.28	2.34	7.34
Min	-2.34	-2.19	-6.23	-2.34	-2.19	-6.60	-4.80	-2.19	-6.60
Mean	0.14	-0.15	0.58	0.08	-0.14	0.86	-0.32	-0.07	0.91
RMS	1.29	1.03	3.29	1.35	1.08	3.45	1.53	1.08	3.46

Figure 9 shows the comparison between the predictions and the true values of GCM in the three directions. The black line in the figure represents the true values of GCM, and the red line represents the predicted values. The statistical results of the prediction precision of the LM+MSSA+ARMA model are shown in the Table 4. As shown in Fig. 8 and Table 4 that the combined model has the best prediction precision when the prediction length is 6 months. The RMSE in X, Y, and Z directions are 1.29 mm, 1.03 mm and 3.29 mm, respectively, and the precision of X and Y directions are all within 1.5 mm. The precision of the Z direction is relatively poor, which may be caused by the large change in the amplitude of GCM in the Z direction. As the prediction time increases, the predicted precision shows a downward trend as a whole, reaching the maximum when the prediction length is 2 years, and the prediction precision in the three directions is 1.53 mm, 1.08 mm and 3.46 mm respectively. In general, the LM+MSSA+ARMA model has good performance in short-term, medium-term and long-term predictions of GCM, and can provide prediction precision of 1.5 mm, 1.1 mm and 3.5 mm in the X, Y and Z directions respectively.

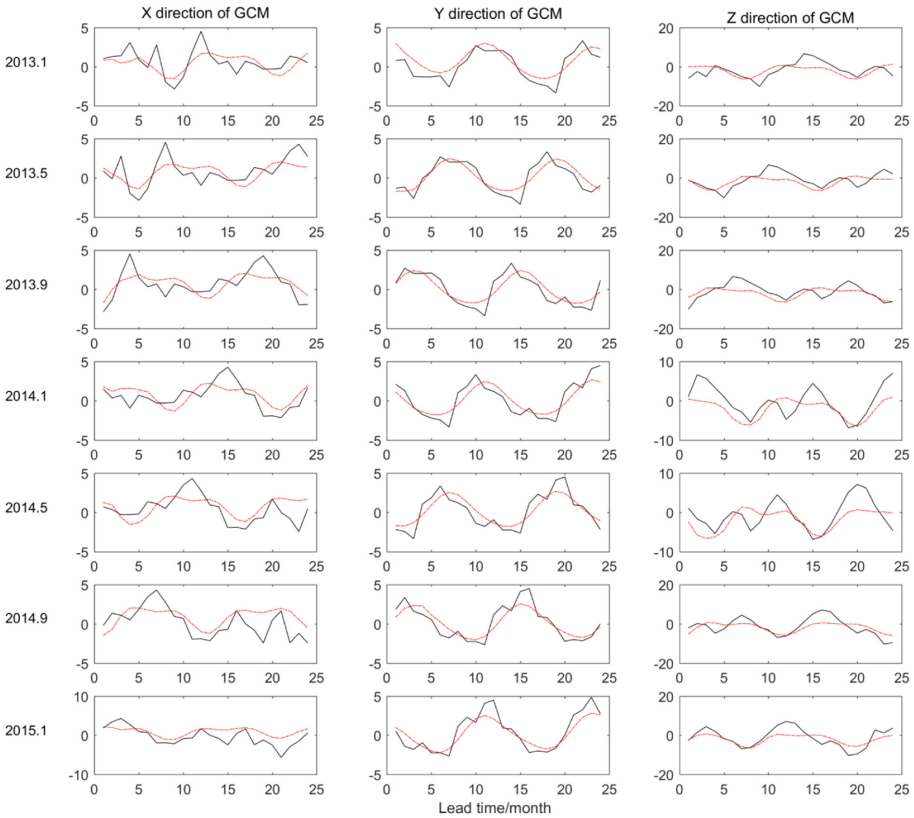


**Fig. 9.** Comparison of GCM predictions

## 5 Conclusions

The GCM products estimated from SLR data released by CSR are analyzed to determine the variation of geocenter motion. MSSA is used to analyze the GCM series in the X, Y and Z directions from 1993 to 2017.2. The seasonal variation periods are 0.99 years, 0.5 years, 0.58 years and 1.47 years, and the long period term is 6.09 years in the X, Y and Z directions, which shows that the MSSA can well display and amplify the main periodic signals of the original time series of GCM. The annual characteristics in the three directions are the most obvious and the wave oscillation is stable. The GCM in the X, Y and Z directions are directly analyzed by using MSSA to determine its trends. The long-term trends of the three directions are 0.05 mm/yr, 0.04 mm/yr and  $-0.10$  mm/yr, respectively. The migration velocity in Z direction is obviously higher than that in X and Y directions, which may be mainly caused by the water mass redistribution in the northern and southern hemispheres.

To obtain high-precision geocentric motion prediction parameters, the method combining LM and MSSA and ARMA models is used to predict GCM with ahead 2 years. The

results show that the LM+MSSA+ARMA model can effectively predict GCM parameters, and can provide prediction precision of 1.5 mm, 1.1 mm and 3.5 mm in X, Y and Z directions, respectively.

**Acknowledgements.** We are very grateful to CSR for providing GCM products (<http://ftp.csr.utexas.edu/pub/slr/geocenter/>). This research is supported by the National Natural Science Foundation of China (Grant Nos. 41774001 & 41704015), the Basic Science and Technology Project of China (Grant No. 2015FY310200).

## References

- Altamimi, Z., Collilieux, X., Metivier, L.: ITRF2008: an improved solution of the international terrestrial reference frame. *J. Geodesy* **85**(8), 457–473 (2011). <https://doi.org/10.1007/s00190-011-0444-4>
- Baur, O., Kuhn, M., Featherstone, W.E.: Continental mass change from GRACE over 2002–2011 and its impact on sea level. *J. Geodesy* **87**(2), 117–125 (2013). <https://doi.org/10.1007/s00190-012-0583-2>
- Blewitt, G.: Self-consistency in reference frames, geocenter definition, and surface loading of the solid Earth. *J. Geophys. Res. Solid Earth* **108**(B2), 2103 (2003). <https://doi.org/10.1029/2002JB002082>
- Blewitt, G., Clarke, P.: Inversion of Earth's changing shape to weigh sea level in static equilibrium with surface mass redistribution. *J. Geophys. Res. Solid Earth* **108**(B6), 2311 (2003). <https://doi.org/10.1029/2002JB002290>
- Blewitt, G., Lavalée, D.E., Clarke, P.J., Nurutdinov, K.: A new global mode of Earth deformation: seasonal cycle detected. *Science* **294**(5550), 2342–2345 (2001). <https://doi.org/10.1126/science.1065328>
- Bouille, F., Cazenave, A., Lemoine, J.M., Cretaux, J.F.: Geocentre motion from the DORIS space system and laser data to the Lageos satellites: comparison with surface loading data. *Geophys. J. Int.* **143**(1), 71–82 (2000). <https://doi.org/10.1046/j.1365-246x.2000.00196.x>
- Cheng, M.K., Tapley, B.D., Ries, J.C.: Deceleration in the Earth's oblateness. *J. Geophys. Res. Solid Earth* **118**(2), 740–747 (2013). <https://doi.org/10.1002/jgrb.50058>
- Cheng, M.K., Ries, J.C., Tapley, B.D.: Geocenter variations from analysis of SLR data. In: IAG Commission Symposium 2010, Reference Frames for Applications in Geosciences (REFAG2010), Mame-La-Vallee, France, 4–8 October 2010, pp. 19–25 (2013b). [https://doi.org/10.1007/978-3-642-32998-2\\_4](https://doi.org/10.1007/978-3-642-32998-2_4)
- Crétaux, J., Soudarin, L., Davidson, F.J.M., Gennero, M., Bergé-Nguyen, M., Cazenave, A.: Seasonal and interannual geocenter motion from SLR and DORIS measurements: comparison with surface loading data. *J. Geophys. Res. Solid Earth* **107**(B12), 2374 (2002). <https://doi.org/10.1029/2002JB001820>
- Dong, D., Dickey, J.O., Chao, Y., Cheng, M.K.: Geocenter variations caused by atmosphere, ocean and surface ground water. *Geophys. Res. Lett.* **24**(15), 1867–1870 (1997). <https://doi.org/10.1029/97GL01849>
- Dong, D., Yunck, T., Hefflin, M.: Origin of the international terrestrial reference frame. *J. Geophys. Res. Solid Earth* **108**(B4), 2200 (2003). <https://doi.org/10.1029/2002JB002035>
- Golyandina, N., Nekrutkin, V., Zhigljavsky, A.: *Analysis of Time Series Structure*. Chapman and Hall/CRC, New York (2001). <https://doi.org/10.1201/9780367801687>
- Feissel-Vernier, M., Le Bail, K., Berio, P., Coulot, D., Ramillien, G., Valette, J.J.: Geocentre motion measured with DORIS and SLR, and predicted by geophysical models. *J. Geodesy* **80**(8), 637–648 (2006). <https://doi.org/10.1007/s00190-006-0079-z>

- Greff-Lefftz, M., Legros, H.: Fluid core dynamics and degree-one deformations: Slichter mode and geocenter motions. *Phys. Earth Planet. Inter.* **161**(3–4), 150–160 (2007). <https://doi.org/10.1016/j.pepi.2006.12.003>
- Guo, J.Y., Han, Y.B., Hwang, C.W.: Analysis on motion of Earth's center of mass observed with CHAMP mission. *Sci. China, Ser. G* **51**(10), 1597–1606 (2008). <https://doi.org/10.1007/s11433-008-0152-0>
- Guo, J.Y., Chang, X.T., Han, Y.B., Sun, J.L.: Periodic geocenter motion measured with SLR in 1993–2006. *Acta Geodaetica et Cartographica Sinica* **38**(4), 311–317 (2009). <https://doi.org/10.3321/j.issn:1001-1595.2009.04.005>
- Hassani, H.: Singular spectrum analysis: methodology and comparison. *J. Data Sci.* **5**(2), 239–257 (2007). <https://mpira.ub.uni-muenchen.de/4991/>
- Klemann, V., Martinec, Z.: Contribution of glacial-isostatic adjustment to the geocenter motion. *Tectonophysics* **511**(34), 99–108 (2011). <https://doi.org/10.1016/j.tecto.2009.08.031>
- Kong, Q., Guo, J., Sun, Y., Zhao, C., Chen, C.: Centimeter-level precise orbit determination for the HY-2A satellite using DORIS and SLR tracking data. *Acta Geophys.* **65**(1), 1–12 (2017). <https://doi.org/10.1007/s11600-016-0001-x>
- Kuzin, S.P., Tatevian, S.K.: Determination of seasonal geocenter variations from DORIS, GPS and SLR data. In: *Proceedings of the Joumees Systemes de Reference Sptio-Temporels2005*, Warsaw, pp. 76–77 (2005)
- Kuzin, S.P., Tatevian, S.K., Valeev, S.G., Fashutdinova, V.A.: Studies of the geocenter motion using 16-years DORIS data. *Adv. Space Res.* **46**(10), 1292–1298 (2010). <https://doi.org/10.1016/j.asr.2010.06.038>
- Metivier, L., Greff-Lefftz, M., Altamimi, Z.: On secular geocenter motion: the impact of climate changes. *Earth Planet. Sci. Lett.* **296**(3–4), 360–366 (2010). <https://doi.org/10.1016/j.epsl.2010.05.021>
- Montag, H.: Geocenter variations derived by different satellite methods. IERS Technical Note25. Paris: Observatoire de Paris, 71–74 (1999)
- Oropeza, V., Sacchi, M.: Simultaneous seismic data denoising and reconstruction via multichannel singular spectrum analysis. *Geophysics* **76**(3), V25–V32 (2011). <https://doi.org/10.1190/1.3552706>
- Pavlis, H.: Fortnightly resolution geocenter series: a combined analysis of Lageos 1 and 2 SLR data (1993–96). IERS Technical Note 25, Paris, Observatoire de Paris, pp. 75–84 (1999)
- Pearlman, M., et al.: Laser geodetic satellites: a high-accuracy scientific tool. *J. Geodesy* **93**(11), 2181–2194 (2019). <https://doi.org/10.1007/s00190-019-01228-y>
- Riddell, A.R., King, M.A., Watson, C.S., Sun, Y., Riva, R.E.M., Rietbroek, R.: Uncertainty in geocenter estimates in the context of ITRF2014. *J. Geophys. Res. Solid Earth* **122**, 4020–4032 (2017). <https://doi.org/10.1002/2016JB013698>
- Ries, J.C.: Reconciling estimates of annual geocenter motion from space geodesy. In: *Proceedings of the 20th International Workshop on Laser Ranging*, Potsdam, Germany, pp. 10–14 (2016)
- Rietbroek, R., Brunnabend, S.E., Kusche, J., Schroter, J.: Resolving sea level contributions by identifying fingerprints in time-variable gravity and altimetry. *J. Geodyn.* **s59-60**(5), 72–81 (2012a). <https://doi.org/10.1016/j.jog.2011.06.007>
- Rietbroek, R., et al.: Global surface mass from a new combination of GRACE, modelled OBP and reprocessed GPS data. *J. Geodyn.* **59-60**(5), 64–71 (2012b). <https://doi.org/10.1016/j.jog.2011.02.003>
- Shen, Y., Guo, J., Liu, X., Wei, X., Li, W.: One hybrid model combining singular spectrum analysis and LS+ARMA for polar motion prediction. *Adv. Space Res.* **59**(2), 513–523 (2017). <https://doi.org/10.1016/j.asr.2016.10.023>
- Shen, Y., Guo, J., Liu, X., Kong, Q., Guo, L., Li, W.: Long-term prediction of polar motion using a combined SSA and ARMA model. *J. Geodesy* **92**(3), 333–343 (2018). <https://doi.org/10.1007/s00190-017-1065-3>



- Sun, Y., Riva, R., Ditmar, P.: Optimizing estimates of annual variations and trends in geocenter motion and  $J(2)$  from a combination of GRACE data and geophysical models. *J. Geophys. Res. Solid Earth* **121**(11), 8352–8370 (2016). <https://doi.org/10.1002/2016JB013073>
- Trupin, A.S., Meier, M.F., Wahr, J.M.: Effect of melting glaciers on the Earth's rotation and gravitational field. *Geophys. J. Int.* **108**(1), 1–15 (1992). <https://doi.org/10.1111/j.1365-246X.1992.tb00835.x>
- Vautard, R., Ghil, M.: Singular spectrum analysis in nonlinear dynamics, with applications to paleo-climatic time series. *Physica D-Nonlinear Phenomena* **35**(3), 395–424 (1989). [https://doi.org/10.1016/0167-2789\(89\)90077-8](https://doi.org/10.1016/0167-2789(89)90077-8)
- Wang, X., Cheng, Y., Wu, S., Zhang, K.: An enhanced singular spectrum analysis method for constructing nonsecular model of GPS site movement. *Journal of Geophysical Research: Solid Earth* **121**(3), 2193–2211 (2016). <https://doi.org/10.1002/2015JB012573>
- Watkins, M.M., Eanes, R.J.: Observations of tidally coherent diurnal and semidiurnal variations in the geocenter. *Geophys. Res. Lett.* **24**(17), 2231–2234 (1997). <https://doi.org/10.1029/97GL52059>
- Wei, N., Shi, C., Liu, J.N.: Effects of surface loading and heterogeneous GPS network on Helmert transformation. *Chin. J. Geophys.* **59**(2), 484–493 (2016). <https://doi.org/10.6038/cig20160208>
- Wu, X., et al.: Simultaneous estimation of global present-day water transport and glacial isostatic adjustment. *Nat. Geosci.* **3**(9), 642–646 (2010). <https://doi.org/10.1038/ngeo938>
- Wu, X., Ray, J., Dam, T.V.: Geocenter motion and its geodetic and geophysical implications. *J. Geodyn.* **58**(3), 44–61 (2012). <https://doi.org/10.1016/j.jog.2012.01.007>
- Zhao, C., Ma, T.: The estimation and prediction of geocenter motion based on GNSS/SLR weekly solutions. In: 42nd COSPAR Scientific Assembly, Pasadena, California, USA, 14–22 July 2018, B2-1 (2018)
- Zhao, C., Qiao, L., MA, T.: Estimation and prediction of geocenter motion based on GNSS weekly solutions of IGS. In: American Geophysical Union, Fall Meeting, San Francisco, California, 9–13 December 2019, G12A-05 (2019)
- Zhou, M.S., Guo, J.Y., Shen, Y., Kong, Q.L., Yuan, J.J.: Extraction of common mode errors of GNSS coordinate time series based on multi-channel singular spectrum analysis. *Chin. J. Geophys.* **61**(11), 4383–4395 (2018). <https://doi.org/10.6038/cjg2018L0710>
- Zotov, L., Bizouard, C.H., Shum, C.K.: About possible interrelation between Earth rotation and climate variability on a decadal time-scale. *Geodesy Geodyn.* **7**(3), 216–222 (2016). <https://doi.org/10.1016/j.geog.2016.05.005>